Fibril Density Reduction in Keratoconic Corneas

Dong Zhou[1], Ahmed Abass[2,3]*, Bernardo Lopes[4,5], Ashkan Eliasy[4], Sally Hayes[6], Craig Boote[6], Keith M Meek[6], Alexander Movchan[1], Natalia Movchan[1], Ahmed Elsheikh[4, 7, 8]

[1] Department of Mathematical Sciences, School of Physical Sciences, University of Liverpool, Liverpool, UK

[2] Department of Mechanical, Materials and Aerospace Engineering, School of Engineering, University of Liverpool, Liverpool, UK

[3] Department of Production Engineering and Mechanical Design, Faculty of Engineering, Port Said University, Egypt

[4] Department of Civil Engineering and Industrial Design, School of Engineering, University of Liverpool, Liverpool, UK

[5] Department of Ophthalmology, Federal University of Sao Paulo – Sao Paulo

[6] School of Optometry and Vision Sciences, Cardiff University, Cardiff, UK

[7] Beijing Advanced Innovation Centre for Biomedical Engineering, Beihang University, Beijing, 100083, China

[8] NIHR Biomedical Research Centre for Ophthalmology, Moorfields Eye Hospital NHS Foundation Trust and UCL Institute of Ophthalmology, London, UK

***Corresponding author:** Dr Ahmed Abass, School of Engineering, University of Liverpool, Liverpool, UK, a.abass@liverpool.ac.uk

Keywords: cornea; keratoconus; tissue microstructure; ocular biomechanics

Word count: 5556

Abstract

This study aims to estimate the reduction in collagen fibril density within the central 6mm radius of keratoconic corneas through processing of microstructure and videokeratography data. Collagen fibril distribution maps and topography maps were obtained for seven keratoconic and six healthy corneas, and topographic features were assessed to detect and calculate the area of the cone in each keratoconic eye. The reduction in collagen fibril density within the cone area was estimated with reference to the same region in the characteristic collagen fibril maps of healthy corneas. Together with minimum thickness and mean central corneal refractive power, the cone area was correlated with the reduction in the cone collagen fibrils. For the corneas considered, the mean area of keratoconic cones was 3.30±1.90 mm^2. Compared with healthy corneas, fibril density in the cones of keratoconic corneas was lower by as much as 35% and the mean reduction was 17±10%. A linear approximation was developed to relate the magnitude of reduction to the refractive power, minimum corneal thickness and cone area (R^2= 0.95, $p< 0.001$). Outside the cone area, there was no significant difference between fibril arrangement in healthy and keratoconic corneas. The presented method can predict the mean fibril density in the keratoconic eye's cone area. The technique can be applied in microstructure-based finite element models of the eye to regulate its stiffness level and the stiffness distribution within the areas affected by keratoconus.

Introduction

Keratoconus (KC) is a bilateral non-inflammatory corneal disease that affects approximately 1 in 2000 of the population (1). The keratoconic cornea progressively develops ectasia with local thinning and a cone-shaped protrusion, which results in visual impairment. The management of KC, including its diagnosis and treatment, has developed significantly in recent decades.

Computer-assisted videokeratography provides quantitative imaging of corneal anterior and posterior topographies. KC can be detected and classified based on corneal topography through clinical signs of disease evolution, index-based classification systems and advanced machine learning algorithms (1-7). These detection techniques are clinically useful to evaluate the stage of KC and guide the selection of suitable treatments.

Corneal shape is the outcome of an equilibrium between the intraocular pressure (IOP) and the mechanical resistance (or stiffness) of ocular tissue. In keratoconic eyes, and in particular within the KC cone, the stiffness of corneal tissue is known to be lower than in healthy corneas due to the combined effect of smaller thickness and softer material (8-12). The reduced stiffness in the cone is thought to be the cause of the distortion of the tissue and the subsequent loss in vision clarity.

While the pathogenesis of KC remains unclear, there is strong evidence that the microstructural alterations in cone tissue, in terms of both collagen fibril density and organisation, are behind the reduced stiffness of KC tissue. Literature in this field shows consistently that healthy corneas have preferential fibril organisation with more fibrils lying in the horizontal and vertical directions than in any other direction in the central region of the cornea; the fibrils then gradually assume an increasingly tangential arrangement with increasing proximity to the limbus (13-15). This arrangement is clearly disturbed in KC eyes and is accompanied by a significant reduction in fibril content (16-18), and a decreased incidence of collagen interlacing between lamellae in the para-apical region (19, 20). These changes cause loss of mechanical cohesiveness, and facilitate slippage between stromal

lamellae (16, 21). Hayes, Boote (18) demonstrated that these effects were concentrated in the area where the KC cone develops with significant local thinning and surface distortion, thus providing evidence of an association between microstructural degradation and topographical distortion.

The last two decades saw several attempts to develop numerical models of ocular biomechanical behaviour based on the tissue's microstructure and in particular its collagen fibril distribution. These models benefitted from the extensive work carried out in X-ray scattering studies to quantify the fibril density and orientation across the cornea (22-26). However, while similar studies have attempted to quantify the microstructural features of KC corneas, no consensus has developed yet on the effect of KC on fibril organisation.

This study attempts to address this shortfall through analysis of microstructure maps of seven KC corneas and six healthy corneas. It seeks to provide an estimate of the reduction in fibril density within the cone area that can be expected in eyes with different disease severity stages, thickness loss and cone surface areas. With this information, progress can be made in building patient-specific, microstructure-based numerical models of the biomechanical behaviour of KC eyes.

Methods

Collagen fibril maps

This study utilised a large collection of previously published x-ray scattering data that was gathered for a number of individual studies (15, 27-29), and done so in accordance with the ethical principles of the declaration of Helsinki and its subsequent revisions, with full, informed consent from the human tissue donors, and with approval from the Human Science Ethical Committee (School of Optometry and Vision Sciences, Cardiff University, UK). This study involved 6 healthy donor corneas (with at least 13 mm of surrounding sclera), collected post-mortem from 4 donors aged between 54 and 75 years. It also included 7 central corneal buttons with severe keratoconus (KC) collected using 7.5 mm diameter trephines from 7

donors aged between 24 and 39 years who underwent penetrating keratoplasty. The patients' demographic characteristics and corneal thickness values are summarised in Table 1.

Table 1 Patients' demographic characteristics including age, gender, left/right eyes.

	Healthy	Keratoconus	
Number of corneas and donors	6, 4	7, 7	
Age in years (mean±SD range)	65.0±8.8 (54 – 75)	30.1±4.4 (24 – 39)	$p < 0.001$
Left:Right eyes ratio	1.0:1.0	1.0:2.5	$p = 0.576$
Male:Female gender ratio	1:1	1:1.3	$p = 1.000$
Central corneal thickness (mean$\pm$std μm)	546.4$\pm$12.5	293.7±88.2	$p < 0.001$

The healthy corneas were obtained within 18 hrs post-mortem, stored at 4°C for transport and subsequently fixed in 4% PFA prior to scanning by wide-angle x-ray scattering (WAXS), while the KC corneas were obtained post-operatively, quickly frozen in liquid Nitrogen and stored at -80ºC until required for data collection. This difference in tissue preparation methods was found earlier to have no significant effect on WAXS data (30).

Thickness measurements were taken in healthy eyes prior to PFA tissue fixation using an ultrasound pachymeter (Pachmate 55; DGH Technologies, Exton, PA) with ±5 μm accuracy (Table 1). The thickness was measured at the centre of each cornea and at intervals of 2.5 mm along 8 meridians. Measurements were taken 3 times at each point and the mean value was used. Recorded standard deviation was less than 10 μm for all pachymetry thickness measurements. Interpolation between these values was then used to estimate the tissue thickness across the whole cornea. On the other hand, the thickness across the surface of keratoconic corneas was obtained directly from the videokeratography images recorded prior to the penetrating keratoplasty (Table 1). The different methods used to measure the thickness were found in the past to produce similar results, and were therefore not expected to make a notable effect on the results of this study (31, 32).

Based on the measured central corneal thickness of the healthy specimens (530-560 μm) and the known relationship between thickness and hydration, the healthy corneas were deemed

to be close to physiological hydration at the time of data collection, and therefore at similar hydration to that of the keratoconus tissue.

The white-to-white (WTW) distance was measured in healthy eyes by a digital calliper (Mitutoyo, Hampshire, UK) with ±20 μm accuracy, while in keratoconic eyes, it was obtained directly from the Orbscan output. The WTW values showed little variation with a mean, standard deviation and range of 12.11±0.46 (11.8-13.1 mm) for all eyes. However, despite this little variation, the sampling distance within every specimen was normalised such that the WTW distance became 12.11 mm.

Due to the large dimensions of the healthy cornea-scleral specimens relative to the size of the specimen holder, it was necessary to flatten the tissue slightly prior to scanning. This was achieved by performing a series of six meridional incisions, extending from the corneal limbus to the outer edge of the sclera (thus avoiding damage to the cornea itself) (15, 27).

Just before testing, the KC corneas were thawed, and both the healthy and KC tissue was wrapped in polyvinylidene chloride catering film to minimise tissue dehydration. Wide angle x-rays scatter (WAXS) patterns were obtained from each specimen in a grid system of 0.5 mm intervals in both horizontal and vertical directions for healthy eyes (27), and 0.25 mm intervals for KC eyes (29). The x-ray scattering images collected at every scanning spot were normalised against the x-ray beam intensity and the x-ray exposure time, and subsequently analysed to determine the orientation of fibrillar collagen at equally-spaced 256 orientations covering 360°, as well as the total collagen x-ray scatter intensity at each sampling position. Assuming hydration is fairly uniform across the cornea, then the total x-ray scattering intensity can be seen as a reasonable representation of the relative mass of collagen at each sampling site within an individual cornea. Fibril density was calculated as the total x-ray scatter intensity divided by the local tissue thickness.

Due to the potential for tissue distortion artefacts close to the cut edges in both the healthy and keratoconus specimens, data obtained within 0.75 mm of the sample edge was excluded from the analysis.

Identification of cone area in KC corneas

Videokeratography scans of the keratoconic buttons were obtained using Orbscan (Bausch & Lomb, Technolas PV, Germany) before the surgery, in which they were removed. These scans provided corneal anterior and posterior topography maps, mean power maps and thickness distribution maps. Central corneal thickness measurements were taken with partial coherence interferometry, ultrasound, and the Orbscan system (33). The topography maps enabled calculation of the height of the cornea relative to a best-fit spherical (BFS) surface, with the highest point assumed to represent the centre of the keratoconic cone (34, 35). The refractive power of healthy corneas P was calculated using the Gaussian optics formula (36-38).

$$P = \frac{n_{cornea} - n_{air}}{R_{anterior}} + \frac{n_{aqueous} - n_{cornea}}{R_{posterior}} - \frac{t_c}{n_{cornea}} \times \frac{n_{cornea} - n_{air}}{R_{anterior}} \times \frac{n_{aqueous} - n_{cornea}}{R_{posterior}} \quad (1)$$

Where the refractive indices of air, n_{air}, cornea, n_{cornea}, and aqueous, $n_{aqueous}$, were set at 1.0, 1.376 and 1.336, respectively following Gullstrand's relaxed eye model (39, 40), and t_c, represented the central corneal thickness. The sagittal radii of curvatures at any point were calculated as:

$$R = \frac{x}{\cos\left(\frac{\pi}{2} - \alpha\right)} \quad (2)$$

where α is the tangent angle at the calculation point and x is the distance from the apex.

The mean power map was constructed based on the average of the two principal curvatures at each scanned point (38).

The boundary of keratoconic cones was detected based on the observation that it coincided with a sudden, abnormal reversal of corneal curvature, Figure 1 & S1. As outlined in our earlier studies (35, 41, 42), corneal profiles along equally-spaced meridian lines originating at the

cone centre and extending outwards were analysed. Initially, a best-fit sphere was fitted to the central, 7 mm diameter area of each corneal anterior surface, and the radial distance from each data point on a corneal surface to the centre of the sphere was calculated. This was followed by subtracting the radius of the sphere from these radial distances and the position and magnitude of the largest positive difference were assumed to point at the location and height of the cone centre, respectively.

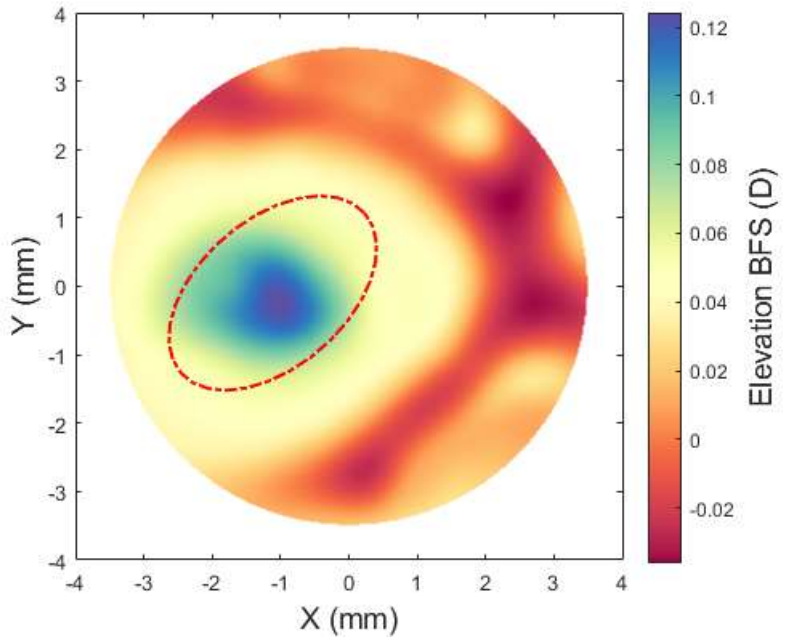

Figure 1: Topography map of the central 7 mm of the keratoconic right eye cornea KC4. The origin (0,0) is the corneal apex and red lines represent the KC cone boundaries.

To estimate the area of pathology, height data relative to the optimal sphere were determined along 360 equally-spaced lines meeting at the cone centre and extending outwards using triangle-based cubic interpolation (43). A first derivative of the height data was calculated to determine the tangent to the surface along these lines. The second derivative was then calculated to represent the rate of change of this gradient. Since the rate of gradient change experiences a change in direction when the point of interest moves from the cone area to the surrounding healthy area, a sudden change in the sign of the rate of change in tangent

gradient is indicative of an intersection with the transition zone between the pathologic area and the remaining corneal tissue. Locating the transition zone between the area of pathology and the remaining corneal tissue using this method then allowed calculating the cone area.

An iterative process was then initiated in which the cone area was removed from the topography data before re-identifying the optimal sphere and repeating the subsequent steps. This process was repeated until the difference between the results (cone height and centre location) of two subsequent analyses became smaller than 1.0 μm.

Fibril density reduction factor 'κ'

Assessment of the reduction in collagen fibril density in KC cones started with developing a map representing the mean density distribution in the six healthy corneas scanned. As it was not possible to scan at exactly the same points in all cornea specimens, as discussed in our previous study Zhou, Eliasy (15), 10th order Zernike polynomials were used to fit the fibril density measurements (ρ) obtained for each cornea:

$$\rho = \sum_{n=0}^{10} \sum_{m=-n:2:n} Z_n^m(r,\theta) C_n^m(\theta) \tag{3}$$

Where Zernike term is represented by

$$Z_n^m(r,\theta) = \begin{cases} R_n^{|m|} cos(m\theta) & m > 0 \\ R_n^{|m|} sin(m\theta) & m < 0 \\ R_n^0 & m = 0 \end{cases} \tag{4}$$

with the radial polynomial $R_n^{|m|}$ defined as

$$R_n^{|m|} = \sum_{i=0}^{\frac{n-|m|}{2}} \frac{(-1)^i (n-i)!\, r^{n-2i}}{i!\,((n+|m|)/2-i)!\,((n-|m|)/2)!}, \qquad (0 \le r \le 1) \tag{5}$$

Where (r,θ) are the polar coordinates of x-ray scanning points, n is the radial order of the polynomial, and m is an azimuthal integer index which varies from -n to n for even m-n while equals 0 for odd n-m.

The average values of Zernike coefficients were then determined and used to represent the mean density distribution for healthy corneas. This process enabled comparison of fibril density in KC corneas (both within and outside cone boundary) with mean fibril density in the corresponding areas of healthy corneas. Therefore, the analysis included two sets of comparisons. First, the fibril density within the cone area in keratoconic corneas was compared to the density in corresponding areas in healthy corneas. The second comparison was between the fibril density outside the cone in keratoconic corneas and the density in corresponding areas in healthy eyes. This exercise led to the development of a fibril density reduction factor ($\boldsymbol{\kappa}$) that quantified the mean reduction in fibril density in each KC cone relative to the corresponding area in healthy corneas:

$$\kappa = \frac{C_k}{C_h}\frac{S_h}{S_k} \tag{6}$$

where, for each KC cone, C_h and S_h are the mean fibril density in the healthy corneal areas that correspond to the areas inside (C) and outside (S) the KC cone, respectively. Likewise, C_k and S_k represent the mean fibril density inside and outside the cone area in each KC cornea. Expressing the fibril reduction factor as a ratio was used to eliminate any hydration-induced variation in absolute collagen scatter caused by the different sample storage methods of KC and healthy corneal specimens.

A stepwise linear regression model was fitted to assess the correlation between κ and topographic features of the cornea including the mean central refractive power (P) obtained within the central 3 mm diameter zone, the minimum corneal thickness (T), the KC cone area (A) and the distance between the cone centre and corneal apex (D). Both P and T were extracted from the Obscan reports. Using the forward stepwise approach, the variables that could explain most of the variance in κ and therefore composed the final model were P, T and A.

The first-order polynomial adopted for the dependence of κ on P, T and A took the following form (the first order was adopted to avoid overfitting, which can be caused by the small size of the database):

$$\kappa = a_1 A + a_2 P + a_3 T + a_4 \quad (7)$$

In Equation 7, a_1 to a_4 are constants, which were optimised using the least square method with the objective function:

$$RMS = \frac{1}{n}\sum_{i=1}^{n}\left(\kappa_{mi} - \kappa_e(A_i, P_i, T_i)\right)^2 \quad (8)$$

Where RMS is the root mean square error, n is the number of data points, κ_{mi} is the measured value of density reduction based on KC fibril map i, and κ_e is the estimated density reduction based on Equation 7. Each KC cornea provided one data point i, and six more points were added to represent the healthy corneas, with $\kappa = 1$, $A = 0$, $P \in [43D, 45D]$, $T \in [530\mu m, 560\mu m]$.

K-fold cross-validation was used to test the accuracy of the linear model in predicting fibril density reduction. Data of one keratoconic cornea was kept in every validation cycle to be used in testing the regression model, while data of other eyes were used in its training and calculating its coefficients. The model finally adopted the average values of coefficients following all K-fold cross-validation steps.

Statistical analysis

Statistical analysis was carried out using the MATLAB and Statistics Toolbox Release 2019b (The MathWorks, Inc., Natick, Massachusetts, United States). The Goodness-of-fit of the regression model relating κ to P, T and A was evaluated with the coefficient of determination (R^2). The closer the R^2 is to 1, the higher the variation of the dependent variable explained by the independent variables in the regression model. The comparison of the continuous variables was performed using either Student's t-test or Mann-Whitney U-test according to the variables' distribution. The categorical variables were compared using the Chi-Squared test. A p-value lower than 0.050 was considered statistically significant.

Results

KC cone area

Figure 2 shows the fibril density maps of the seven keratoconic corneas with the estimated cone boundary marked in each case. The cone area (A), the central refractive power (P), the minimum thickness (T), and the fibril reduction factor (κ) measured from the fibril density maps are also listed in Table 2. The results show trends in which increases in cone area or mean power, or decreases in min thickness were associated with higher fibril density reductions (i.e. smaller κ). However, despite the significant correlation between κ and each of A, P and T, there was no correlation between A and P (p= 0.37), A and T (p= 0.89), or R and T (p= 0.18).

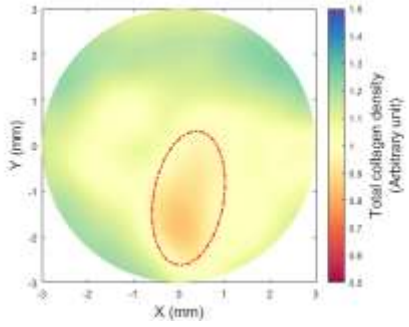

(a) KC1, Left

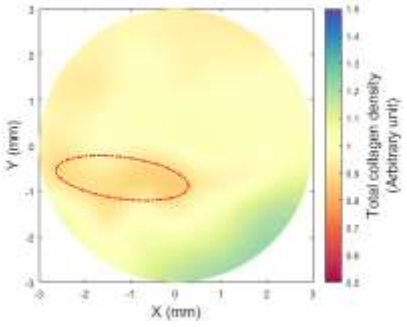

(b) KC2, Right

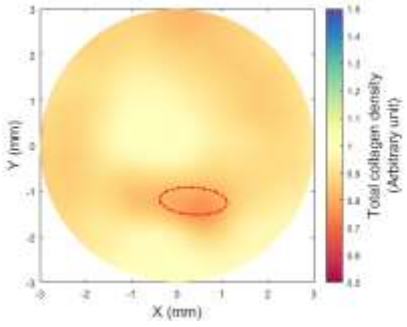

(c) KC3, Right

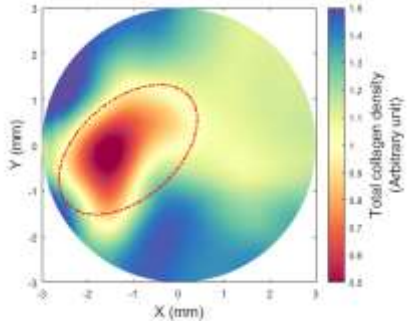

(d) KC4, Right

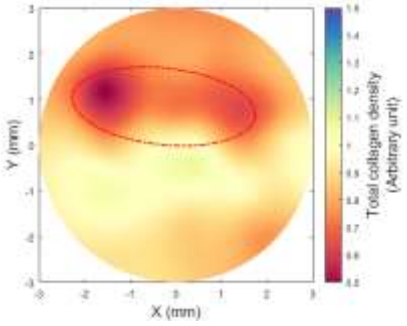

(e) KC5, Right

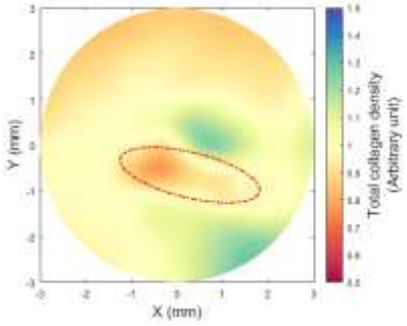

(f) KC6, Left

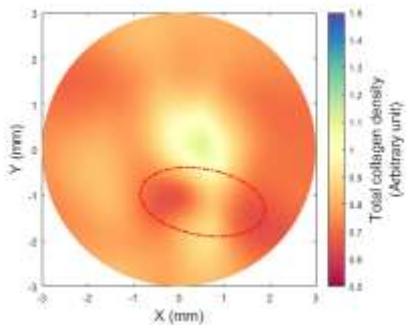

(g) KC7, Right

Figure 2 Fibril density maps for seven keratoconic corneas. The origin (0,0) is the corneal apex. Red lines represent the KC cone boundaries.

Table 2 Measurements of cone area, mean central refractive power, minimum thickness and cone fibril density reduction in keratoconic corneas

Specimen	Cone area, A (mm^2)	Mean power, P (Diopter)	Min Thickness, T (μm)	Fibril reduction factor, κ
KC1	3.61	46.90	483.0	0.84
KC2	2.18	49.20	220.0	0.90
KC3	0.72	54.30	298.0	0.91
KC4	6.24	58.30	277.0	0.65
KC5	5.17	59.30	279.0	0.73
KC6	2.07	63.20	227.0	0.89
KC7	3.12	63.20	272.0	0.87
Mean±SD (min-max)	3.30±1.90 (0.72-6.24)	56.34±6.47 (46.90-63.20)	293.7±88.2 (220.0-483.0)	0.83±0.10 (0.65-0.91)

Fibril distribution comparisons

The effect of KC on fibril distribution outside the cone area was studied with reference to the results in Figure 3. In this figure, the proportion of collagen fibrils in the 45° sectors surrounding the horizontal and vertical directions, and the tangential direction to the cornea edge was quantified within successive tissue rings, each with 0.5 mm width. All the x-ray scanning points in the healthy cornea maps were included in the calculations while the cone areas were

excluded from the KC cornea calculations. The results covered the central zones with 3 mm radius in KC corneas and 6 mm radius in healthy corneas.

The central corneas within 3 mm radius had percentages of horizontal and vertical fibril contents between 30% and 35% of total density in both healthy and KC eyes. No significant differences were found in percentages of preferentially aligned horizontal fibrils (p= 0.29) or vertical fibrils (p= 0.22) between healthy and KC corneas. Similarly, there were no significant differences between healthy and KC corneas in the percentages of tangential fibrils – mean values ranged between 24 and 28% in both specimen groups.

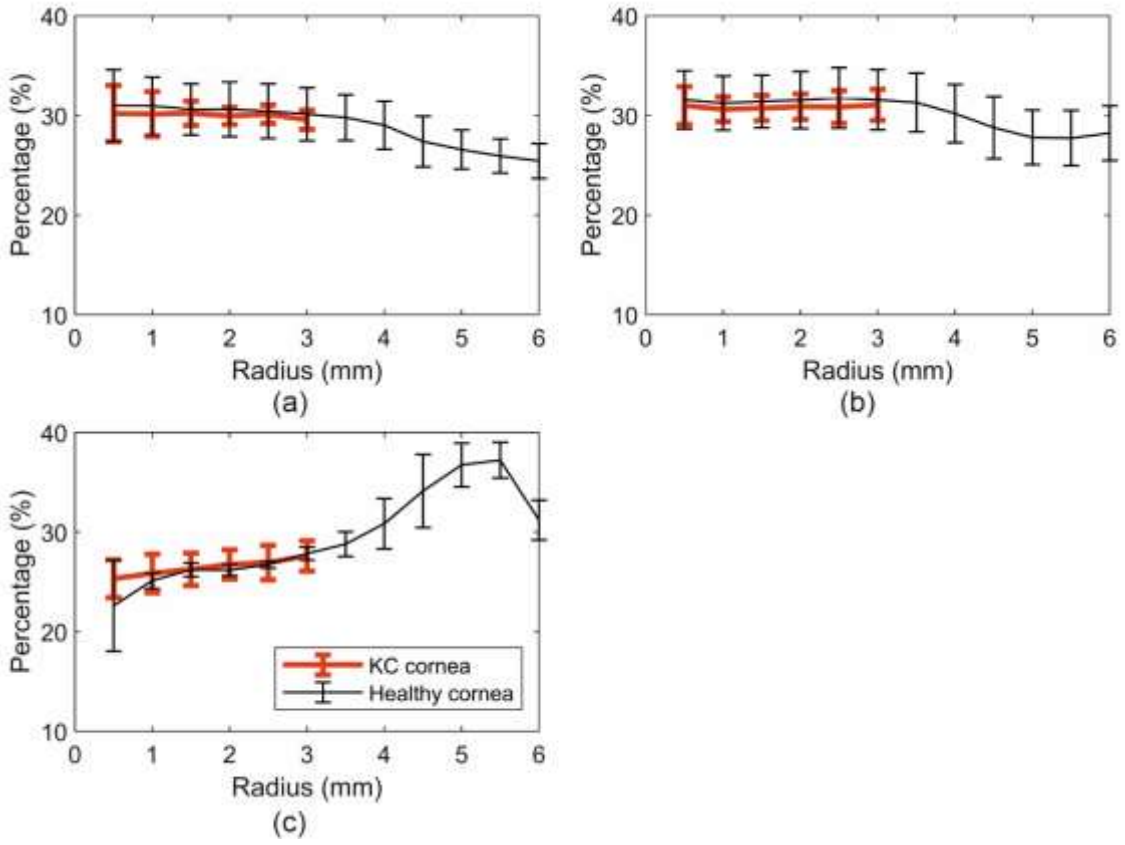

Figure 3 Percentage of fibril quantity in (a) the horizontal direction, (b) the vertical direction, and (c) the tangential direction in healthy and keratoconic cornea specimens.

Fibril density reduction factor 'κ'

Values of constants a_1 to a_4 in the linear relationship between κ and A, P and T, were determined using the least square method as:

$$\kappa = -0.0425A - 0.0004P + 0.0001T + 0.9727 \quad (9)$$

The relationship reflected a decrease in κ (denoting a larger fibril density reduction) with lower minimum corneal thickness (T) (p=0.015), larger central refractive power (P) (p=0.003) and larger cone area (A) (p<0.001). The R^2-value was 0.95 (p< 0.001) and indicated the strong fit of Equation 9 to the measured fibril density measurements. The K-fold cross-validation showed 2.00% error in average fibril reduction in training the model and 2.58% in its testing.

Discussion

Microstructural abnormality in the KC cornea including irregular fibril arrangement, reduced fibril density, lamellae splitting and decreased lamella interweaving was observed in previous studies (16-18, 21, 44). These microstructural changes lead to deterioration in mechanical stiffness compared with the levels expected in healthy corneas (11, 45). The evident association between the reduced fibril density and the stiffness deterioration has enabled the development of numerical models of KC corneas that consider changes in fibril arrangement (22, 23, 25, 26, 28). However, what remains lacking are methods to estimate reductions in fibril density in individual eyes, which would be needed in construction of customised numerical models of KC corneas. This study seeks to address this gap through developing a relationship between fibril density reduction within the cone and a number of corneal features including the cone area, the mean refractive power and the minimum corneal thickness. The study also attempts to establish the effect of keratoconus on the density and distribution of collagen fibrils outside the cone.

As we have shown here, and has been well documented previously (19, 29, 46, 47) in the central region of the healthy cornea most collagen lies in the vertical and horizontal directions

(with ~30% of the total collagen lying in each of the directions (48). It has been suggested that this arrangement of collagen directed towards the insertion points of the rectus muscles may play a biomechanical role in helping the cornea to resist the forces acting upon it and enabling it to maintain its correct curvature. With increasing proximity to the limbus, a transition zone between the cornea and the less curved sclera, the predominant orientation of the collagen becomes increasingly tangential to the edge of the cornea. Although comparative data was not available from the KC corneas beyond a radius of 3 mm, our current study has shown that in the central region of the KC corneas (with the exclusion of the cone areas), the proportion of collagen aligned in the vertical and horizontal directions fibrils did not differ significantly from that of the healthy corneas.

The range of fibril density reduction in the cone areas of the 7 KC corneas analysed in this study was between 20 and 39%. This magnitude of density loss was correlated with three parameters; namely the cone area, the mean refractive power and the minimum corneal thickness ($p= 0.001$, 0.008, 0.041, respectively). Another parameter, the distance between corneal apex and cone centre, was excluded due to lack of significant correlation with density reduction. Based on these results, an estimate of a cone fibril reduction factor κ was developed and found to offer a close match with measured values. With the proven dependence of corneal stiffness on collagen fibril distribution, this parameter could be employed in numerical analyses to simulate the effect of KC on corneal biomechanical behaviour.

The study has a number of limitations. First, due to the low intensity of collagen x-ray scatter (and the resulting poor signal to noise ratio) from the cone region of the keratoconus corneas, coupled with the lack of inter-specimen consistency in terms of collagen orientation in this region, it was not feasible to include the cone region in our current analysis. Second, the number of cornea specimens included in the study was relatively small due to the difficulty in obtaining full tissue thickness KC buttons. As new data becomes available, the method developed in this study will be updated.

In conclusion, this study presented a method to estimate the reduction in collagen fibril density inside the cone areas of KC corneas. The study also presented evidence that the fibril distribution outside the cone areas was not affected by KC development and progression and was therefore similar to the fibril distribution in healthy corneas. These findings would make it possible to develop customised numerical models that predict the biomechanical behaviour of KC corneas.

Author Contributions Statement

DZ, AA and BL developed the method and drafted the manuscript. DZ, AA and AEliasy performed the analysis. BL performed the statistical analysis. SH, KM and CB collected the x-ray scattering data. AA, AM, NM and AElsheikh supervised the project. AElsheikh designed the study. DZ, AA, SH, KM, CB and AElsheikh revised the manuscript. All authors reviewed the manuscript.

Acknowledgements

Authors acknowledge the EPSRC grant EP/N014499/1, the MRC grants MR/S037829/1, MR/K000837/1, and NIH grant R01EY021500. Authors thank the Diamond Light Source for beamtime access under award numbers MX8443 and MX11316.

Conflict of Interest Statement

There is no conflict of interest to declare.

References:

1. Auffarth GU, Wang L, Völcker HE. Keratoconus evaluation using the Orbscan topography system. Journal of Cataract & Refractive Surgery. 2000;26(2):222-8.
2. Montalbán R, Alio JL, Javaloy J, Piñero DP. Comparative analysis of the relationship between anterior and posterior corneal shape analyzed by Scheimpflug photography in normal and keratoconus eyes. Graefe's Archive for Clinical and Experimental Ophthalmology. 2013;251(6):1547-55.
3. Tomidokoro A, Oshika T, Amano S, Higaki S, Maeda N, Miyata K. Changes in anterior and posterior corneal curvatures in keratoconus. Ophthalmology. 2000;107(7):1328-32.
4. Alió JL, Shabayek MH. Corneal higher order aberrations: a method to grade keratoconus. Journal of Refractive Surgery. 2006;22(6):539-45.
5. Accardo PA, Pensiero S. Neural network-based system for early keratoconus detection from corneal topography. Journal of biomedical informatics. 2002;35(3):151-9.
6. Yousefi S, Yousefi E, Takahashi H, Hayashi T, Tampo H, Inoda S, et al. Keratoconus severity identification using unsupervised machine learning. PLoS One. 2018;13(11):e0205998.
7. Krumeich JH, Daniel J. Lebend-Epikeratophakie und Tiefe Lamelläre Keratoplastik zur Stadiengerechten chirurgischen Behandlung des Keratokonus (KK) I-III. Klinische Monatsblätter für Augenheilkunde. 1997;211(08):94-100.
8. Andreassen TT, Hjorth Simonsen A, Oxlund H. Biomechanical properties of keratoconus and normal corneas. Experimental Eye Research. 1980;31(4):435-41.
9. Scarcelli G, Besner S, Pineda R, Yun SH. Biomechanical Characterization of Keratoconus Corneas Ex Vivo With Brillouin MicroscopyEvaluation of Brillouin Microscopy for Keratoconus. Investigative Ophthalmology & Visual Science. 2014;55(7):4490-5.
10. Reinstein DZ, Gobbe M, Archer TJ, Silverman RH, Coleman DJ. Epithelial, stromal, and total corneal thickness in keratoconus: three-dimensional display with artemis very-high frequency digital ultrasound. Journal of Refractive Surgery. 2010;26(4):259-71.
11. Mikula E, Winkler M, Juhasz T, Brown DJ, Shoa G, Tran S, et al. Axial mechanical and structural characterization of keratoconus corneas. Experimental Eye Research. 2018;175:14-9.
12. Nash IS, Greene PR, Foster CS. Comparison of mechanical properties of keratoconus and normal corneas. Experimental eye research. 1982;35(5):413-24.
13. Aghamohammadzadeh H, Newton RH, Meek KM. X-Ray Scattering Used to Map the Preferred Collagen Orientation in the Human Cornea and Limbus. Structure. 2004;12(2):249-56.
14. Meek K. The cornea and sclera. Collagen: structure and mechanics. 2008:359-96.
15. Zhou D, Eliasy A, Abass A, Markov P, Whitford C, Boote C, et al. Analysis of X-ray scattering microstructure data for implementation in numerical simulations of ocular biomechanical behaviour. PLOS ONE. 2019;14(4):e0214770.
16. Daxer A, Fratzl P. Collagen fibril orientation in the human corneal stroma and its implication in keratoconus. Investigative ophthalmology & visual science. 1997;38(1):121-9.
17. Meek KM, Tuft SJ, Huang Y, Gill PS, Hayes S, Newton RH, et al. Changes in collagen orientation and distribution in keratoconus corneas. Investigative ophthalmology & visual science. 2005;46(6):1948-56.
18. Hayes S, Boote C, Tuft SJ, Quantock AJ, Meek KM. A study of corneal thickness, shape and collagen organisation in keratoconus using videokeratography and X-ray scattering techniques. Experimental Eye Research. 2007;84(3):423-34.
19. Radner W, Zehetmayer M, Skorpik C, Mallinger R. Altered organization of collagen in the apex of keratoconus corneas. Ophthalmic research. 1998;30(5):327-32.
20. Morishige N, Wahlert AJ, Kenney MC, Brown DJ, Kawamoto K, Chikama T-i, et al. Second-Harmonic Imaging Microscopy of Normal Human and Keratoconus Cornea. Investigative Ophthalmology & Visual Science. 2007;48(3):1087-94.

21. Dawson DG, Randleman JB, Grossniklaus HE, O'Brien TP, Dubovy SR, Schmack I, et al. Corneal Ectasia After Excimer Laser Keratorefractive Surgery: Histopathology, Ultrastructure, and Pathophysiology. Ophthalmology. 2008;115(12):2181-91.e1.
22. Pinsky PM, van der Heide D, Chernyak D. Computational modeling of mechanical anisotropy in the cornea and sclera. Journal of Cataract \& Refractive Surgery. 2005;31(1):136-45.
23. Studer H, Larrea X, Riedwyl H, Büchler P. Biomechanical model of human cornea based on stromal microstructure. Journal of biomechanics. 2010;43(5):836-42.
24. Pandolfi A, Manganiello F. A model for the human cornea: constitutive formulation and numerical analysis. Biomechanics and modeling in mechanobiology. 2006;5(4):237-46.
25. Pandolfi A, Holzapfel GA. Three-dimensional modeling and computational analysis of the human cornea considering distributed collagen fibril orientations. Journal of biomechanical engineering. 2008;130(6):061006.
26. Whitford C, Studer H, Boote C, Meek KM, Elsheikh A. Biomechanical model of the human cornea: Considering shear stiffness and regional variation of collagen anisotropy and density. Journal of the mechanical behavior of biomedical materials. 2015;42:76-87.
27. Pijanka JK, Abass A, Sorensen T, Elsheikh A, Boote C. A wide-angle X-ray fibre diffraction method for quantifying collagen orientation across large tissue areas: application to the human eyeball coat. Journal of Applied Crystallography. 2013;46(5):1481-9.
28. Zhou D, Abass A, Eliasy A, Studer HP, Movchan A, Movchan N, et al. Microstructure-based numerical simulation of the mechanical behaviour of ocular tissue. Journal of The Royal Society Interface. 2019;16(154):20180685.
29. Hayes S, Boote C, Tuft SJ, Quantock AJ, Meek KM. A study of corneal thickness, shape and collagen organisation in keratoconus using videokeratography and X-ray scattering techniques. Experimental Eye Research Journal. 2007;84(3):423-34.
30. Boote C, Dennis S, Huang Y, Quantock AJ, Meek KM. Lamellar orientation in human cornea in relation to mechanical properties. J Struct Biol. 2005;149(1):1-6.
31. Sadoughi MM, Einollahi B, Einollahi N, Rezaei J, Roshandel D, Feizi S. Measurement of central corneal thickness using ultrasound pachymetry and Orbscan II in normal eyes. Journal of ophthalmic & vision research. 2015;10(1):4.
32. Rainer G, Findl O, Petternel V, Kiss B, Drexler W, Skorpik C, et al. Central corneal thickness measurements with partial coherence interferometry, ultrasound, and the Orbscan system. Ophthalmology. 2004;111(5):875-9.
33. Dutta D, Rao HL, Addepalli UK, Vaddavalli PK. Corneal thickness in keratoconus: comparing optical, ultrasound, and optical coherence tomography pachymetry. Ophthalmology. 2013;120(3):457-63.
34. Mahmoud AM, Roberts CJ, Lembach RG, Twa MD, Herderick EE, McMahon TT. CLMI: the cone location and magnitude index. Cornea. 2008;27(4):480-7.
35. Eliasy A, Abass A, Lopes BT, Vinciguerra R, Zhang H, Vinciguerra P, et al. Characterization of cone size and centre in keratoconic corneas. Journal of The Royal Society Interface. 2020;17(169):20200271.
36. Olsen T. On the calculation of power from curvature of the cornea. The British Journal of Ophthalmology. 1986;70(2):152-4.
37. Ho J-D, Tsai C-Y, Tsai RJ-F, Kuo L-L, Tsai IL, Liou S-W. Validity of the keratometric index: Evaluation by the Pentacam rotating Scheimpflug camera. Journal of Cataract & Refractive Surgery. 2008;34:137-45.
38. Abass A, Clamp J, Bao F, Ambrosio R, Jr., Elsheikh A. Non-Orthogonal Corneal Astigmatism among Normal and Keratoconic Brazilian and Chinese populations. Curr Eye Res. 2018:1-8.
39. Smit G, Atchison DA. The eye and visual optical instruments. Cambridge, UK: Cambridge University Press; 1970.
40. Vojnikovi Bo, Tamajo E. Gullstrand's Optical Schematic System of the Eye Modified by Vojnikovi & Tamajo. Coll Antropol. 2013;37 (1):41-5.

41. Abass A, Lopes BT, Eliasy A, Wu R, Jones S, Clamp J, et al. Three-dimensional non-parametric method for limbus detection. PLOS ONE. 2018;13(11):e0207710.
42. Abass A, Lopes BT, Eliasy A, Salomao M, Wu R, White L, et al. Artefact-free topography based scleral-asymmetry. PLOS ONE. 2019;14(7):e0219789.
43. Renka RJ, Renka RL, Cline AK. A TRIANGLE-BASED C^1 INTERPOLATION METHOD. The Rocky Mountain Journal of Mathematics. 1984;14(1):223-37.
44. Mathew JH, Goosey JD, Söderberg PG, Bergmanson JP. Lamellar changes in the keratoconic cornea. Acta ophthalmologica. 2015;93(8):767-73.
45. Gefen A, Shalom R, Elad D, Mandel Y. Biomechanical analysis of the keratoconic cornea. Journal of the Mechanical Behavior of Biomedical Materials. 2009;2(3):224-36.
46. Aghamohammadzadeh H, Newton RH, Meek KM. X-ray scattering used to map the preferred collagen orientation in the human cornea and limbus. Structure. 2004;12(2):249-56.
47. Meek KM, Tuft SJ, Huang Y, Gill PS, Hayes S, Newton RH, et al. Changes in collagen orientation and distribution in keratoconus corneas. Investigative ophthalmology & visual science. 2005;46(6):1948-56.
48. Boote C, Dennis S, Huang Y, Quantock AJ, Meek KM. Lamellar orientation in human cornea in relation to mechanical properties. Journal of structural biology. 2005;149(1):1-6.

516 **Supplementary material (S1)**

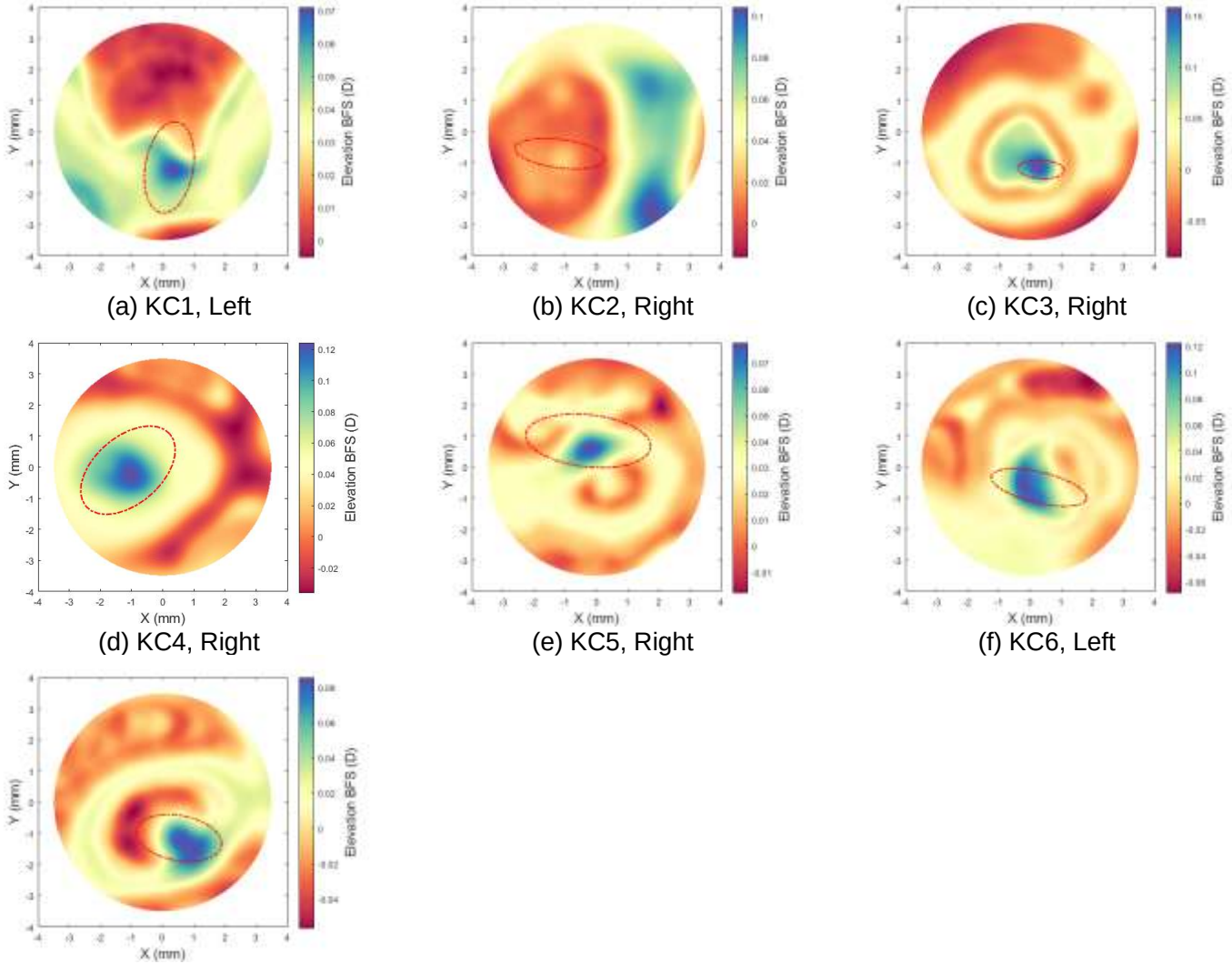

(a) KC1, Left (b) KC2, Right (c) KC3, Right

(d) KC4, Right (e) KC5, Right (f) KC6, Left

(g) KC7, Right

517

518 Figure 1S: Topography maps for the keratoconic corneas included in the current study. The
519 origin (0,0) represents corneal apex, and the red lines represent the keratoconus cone
520 boundaries.

521